STAP FOR CLUTTER AND INTERFERENCE CANCELLATION IN A HF RADAR SYSTEM

Giuseppe A. Fabrizio, Gordon J. Frazer and Mike D. Turley

Defence Science and Technology Organization, AUSTRALIA

ABSTRACT

An alternative skywave line-of-sight (SkyLOS) high frequency radar architecture has been proposed for early detection and tracking of ballistic missiles. It consists of a skywave over-the-horizon (OTH) radar augmented by one or more ground-based systems for *line-of-sight* reception in the illuminated region. The line-of-sight systems provide additional Doppler-time profiles of the target *with different observation geometry* to improve flight trajectory estimation. Targets compete for detection against powerful clutter and interference from man-made and natural sources. We introduce a practical STAP technique to deal with operational signal environments and demonstrate its performance on live SkyLOS data.

1. INTRODUCTION

The SkyLOS system exploits the reflective properties of the ionosphere in the high frequency (HF) band (3-30 MHz) to achieve early detection and tracking of targets at relatively low cost [1]. However, the same mechanism also allows radio frequency interference (RFI) to propagate long distances and potentially impair radar performance. While every attempt is made to select clear frequency channels not occupied by other users, it is impossible to avoid RFI completely by frequency-hopping since natural sources (e.g. lightning) and man-made sources may overlap the receiver bandwith intermittently in an unpredictable manner.

This motivates the use of space-time adaptive processing (STAP) with spatial degrees of freedom to cancel sidelobe RFI [2] and fast-time degrees of freedom to reject main beam RFI that is correlated in range [3]. STAP can also be used to mitigate spread Doppler clutter in velocity bins that contain targets. Due to the very high power of the direct wave at the SkyLOS receiver, this phenomenon can arise from spectral impurities of the radiated waveform and temporal signal distortion caused by the dynamic ionospheric reflection process.

Unlike traditional STAP algorithms where K spatial taps and L temporal taps results in a filter dimension equal to the product KL, we propose an alternative STAP formulation that uses K beams for spatial adaptation and L ranges for fast-time adaptation with the latter taken *only from the reference beam*. The STAP filter dimension is then the addition $Q = K + L$ which is typically much less than the product $Q << KL$. The benefits include the reduced need for statistically homogeneous training data (sample support) and lower computational load for real time implementation.

Thanks to the Radio Frequency Projects Group in ISRD, DSTO Edinburgh, for making the experimental data available.

The data collection procedure is described in section 2. Section 3 explains the conventional signal processing scheme and STAP technique, while section 4 presents experimental results. Conclusions are given in section 5.

2. DATA COLLECTION

The SkyLOS trials data used for this study were collected between 04:45-05:15 UT, 17 April 2004, on a two-dimensional (L-shaped) antenna array located near Darwin in Northern Australia. The array consists of 16 vertically polarized “whip” antenna elements with the 8 elements on each arm uniformly spaced 8 m apart. The output of each antenna element was connected to a separate HF receiver with high dynamic range to allow digital beam steering in azimuth and elevation.

A high power over-the-horizon (OTH) radar transmitter located 1850 km south-east of the receiving array illuminated the Darwin region to allow line-of-sight reception of targets in this area. The trial involved a cooperative aircraft target, shown in Fig.1, that flew out from Darwin in a North-West direction to a range of approximately 400 km. The aircraft was equipped with a GPS logger so that its range, bearing and bi-static Doppler shift could be determined during the flight. At the cruising altitude of 31000 ft, the target falls below the geometrical horizon at a range of about 350 km.

The radar used a linear frequency modulated continuous waveform (FMCW) with carrier frequency $f_c = 19.380$ MHz, bandwidth $f_b = 20$ kHz, and pulse repetition frequency $f_p = 62.5$ Hz. The coherent integration time (CIT) was approximately 4 seconds (i.e. 248 pulses long). A HF spectrum watcher was used to monitor channel occupancy, it indicated that the carrier frequency was unoccupied by other users.

3. STAP TECHNIQUE

After performing standard range-Doppler processing on the digital output of each receiver, conventional (matched filter) beamforming is applied to steer the array at a desired azimuth θ and elevation ϕ. The N-dimensional array steering vector

1-4244-0469-X/06/$20.00

$\mathbf{s}(\theta, \phi)$ used to combine the receiver outputs is given by:

$$\mathbf{s}(\theta, \phi) = [e^{j\mathbf{k}(\theta,\phi)\cdot\mathbf{r}_1}, e^{j\mathbf{k}(\theta,\phi)\cdot\mathbf{r}_2}, \ldots, e^{j\mathbf{k}(\theta,\phi)\cdot\mathbf{r}_N}]^T \quad (1)$$

where $\mathbf{k}(\theta, \phi) = \frac{2\pi}{\lambda}[\cos(\phi)\cos(\theta),\ \cos(\phi)\sin(\theta),\ \sin(\phi)]^T$ is wavevector in the steer direction, $\mathbf{r}_n = [x_n, y_n, z_n]^T$ is the position vector of the n^{th} antenna element relative to the reference for $n = 1, 2, \ldots, N$ and T denotes transpose. Let $\mathbf{x} = [x_1, x_2, \ldots, x_N]^T$ be the array snapshot sampled at a particular range-Doppler cell. For a direction (θ_o, ϕ_o), the conventional output is given by $y_c = \mathbf{s}^H(\theta_o, \phi_o)\mathbf{x}$, where H denotes conjugate transpose. A beam-range-Doppler (BRD) map results for each steer direction, and this data cube is then passed on for CFAR processing and threshold detection.

Our STAP method is applied directly to the conventional BRD data cube. To describe the implementation, we define $\mathbf{z} = [y_c, \mathbf{b}^T, \mathbf{r}^T]^T$ as the STAP data vector used to test for target presence in the same BRD position as the conventional output y_c. This vector contains y_c, a set of K auxiliary beam outputs $\mathbf{b} = [b_1, b_2, \ldots, b_K]^T$ taken from the same range-Doppler cell as the sample y_c but in different beams, and a set of L auxiliary range outputs $\mathbf{r} = [r_1, r_2, \ldots, r_L]^T$ taken from the same beam-Doppler cell as the sample y_c but at different range cells. This allows for joint spatial and fast-time adaptation but only requires $Q = K + L$ degrees of freedom (DOF) as opposed to KL often adopted by STAP approaches [4].

Naturally, the useful signal steering vector needs to be modified according the beam and range transformations and to reflect the chosen set of auxiliary beams and ranges in the data vector $\mathbf{z}$. Define $\mathbf{T}_b$ as the $K \times N$ transformation matrix from the receiver outputs to the selected auxiliary beams, so the modification to the spatial steering vector is given by:

$$\mathbf{v}_b = \mathbf{T}_b\mathbf{s}(\theta_o, \phi_o) \quad (2)$$

Similarly, if there are M fast-time samples per pulse and we define $\mathbf{T}_r$ as the $L \times M$ matrix that transforms these fast-time samples to the selected auxiliary range cells, the modification to the temporal steering vector is given by:

$$\mathbf{v}_r = \mathbf{T}_r\mathbf{g}(t - \tau_o) \quad (3)$$

where $\mathbf{g}(t - \tau_o)$ is the digitized radar waveform delayed by τ_o that corresponds to the range cell under test (i.e. the one corresponding to the sample y_c).

The appropriate steering vector may then be constructed as $\mathbf{v} = [1, \mathbf{v}_b^T, \mathbf{v}_r^T]^T$. Note that this steering vector represents the target structure searched for in the data vector $\mathbf{z}$, and is valid for all Doppler frequency bins at the beam-range cell being tested. If the statistically expected covariance matrix $\mathbf{R} = \mathrm{E}\{\mathbf{z}\mathbf{z}^H\}$ under the null hypothesis were known (i.e. useful signal absent), the optimal STAP weight vector $\mathbf{w}_{opt}$ for the test cell is given by the well known rule:

$$\mathbf{w}_{opt} = \frac{\mathbf{R}^{-1}\mathbf{v}}{\mathbf{v}^H\mathbf{R}^{-1}\mathbf{v}} \quad (4)$$

However, this matrix is not known and must be estimated from a limited set of P (target-free) secondary data vectors $\mathbf{z}_d$ for $d = 1, 2, \ldots, P$ that are presumed to have the same statistical characteristics as the disturbance in the test cell. In our case, the use of Doppler bins immediately neighboring the test cell (and guard cells either side of it) is justified as spread-Doppler clutter and RFI in the test cell also occupies adjacent Doppler cells but the target will be absent. Hence, the actual STAP weights $\hat{\mathbf{w}}$ can be formed by replacing the unknown matrix with its sample estimate $\hat{\mathbf{R}}$ as in the SMI technique [5].

$$\hat{\mathbf{w}} = \frac{\hat{\mathbf{R}}^{-1}\mathbf{v}}{\mathbf{v}^H\hat{\mathbf{R}}^{-1}\mathbf{v}}\ , \quad \hat{\mathbf{R}} = \frac{1}{P}\sum_{d=1}^{P}\mathbf{z}_d\mathbf{z}_d^H \quad (5)$$

These weights are then applied to the test data to obtain the STAP output $y_a = \hat{\mathbf{w}}^H\mathbf{z}$ that may be directly compared with the conventional output y_c. The question then arises as to how the auxiliary beams and ranges are chosen, and also the location and number of the Doppler training cells.

To indicate the background disturbance level at each range after conventional processing, the auxiliary beams are ranked according to the median Doppler spectrum values. Auxiliary beams with higher disturbance levels are chosen in preference to those with lower power. The auxiliary ranges are selected in the immediate neighborhood of the test range as these cells are likely to contain disturbances most correlated with that in the test cell. The total number of DOF Q should be set with consideration to finite sample support (i.e. limited number of Doppler cells available for training) and computational load. Whereas the partitioning $Q = K + L$ into K spatial and L temporal taps should reflect the correlation characteristics of the disturbance. The latter is often unknown and some degree of experimentation is required.

In the next section we illustrate experimental results obtained using $K = 8$ auxiliary beams and $L = 4$ auxiliary ranges. The auxiliary beams steered at the target elevation and are spaced by 10 degrees in azimuth such that they straddle the reference beam. This provides a STAP dimension of $Q = 12$, for which the number of training doppler cells was set to $P = 4Q = 48$. Doppler cells closest to the test cell (and two Doppler guard cells either side of it) were chosen for training. If a cell coincided with the region dominated by powerful direct wave and ground clutter near 0 Hz, the cell was skipped in preference of further cells that were less likely to bias the filter estimate. Using more Doppler cells was possible (i.e 248 cells available in a 4 s CIT) but the statistical benefits gained may be outweighed by the extra risk of including outliers or forms of non-homogeneity in the estimate.

4. EXPERIMENTAL RESULTS

Fig.2(a) shows the range-Doppler map for a particular CIT at the output of a conventional beam steered in the direction of the cooperative target. The target azimuth and elevation were determined from the GPS data and known cruising altitude. In this map, Doppler bins are arranged horizontally and range bins appear vertically. High power is depicted by red, while low power is depicted in blue. This CIT is representative of data collected during intervals deemed to be free of strong RFI. The known target range and Doppler offset allows it to be clearly identified in Fig.2(a). In addition to the strong clutter near 0 Hz, spread Doppler clutter is also quite evident and contributes to raising the apparent"noise floor" over the entire velocity search space.

A cell averaging CFAR method, not discussed here for brevity, is applied to suppress false alarms due to clutter such that targets can be detected with a fixed threshold setting over the entire map. The CFAR processed data at the input to the threshold detection circuit is shown in Fig.2(b). In the same format, Figs.3(a) and 3(b) shows the STAP output for the same data before and after CFAR processing respectively.

A comparison of Fig.2 and Fig.3 clearly shows that the unwanted clutter and noise are better cancelled by STAP. This enables the known target, and a potential target of opportunity at lower range, to be distinguished from the residual clutter and noise background more easily. The target of opportunity is unconfirmed and is not considered further. To quantify the effective improvement in signal-to-noise ratio (SNR) prior to threshold detection, Fig.5(a) compares the conventional and STAP Doppler spectra after CFAR at the target range bin. The STAP improvement in SNR is a significant 6 dB, although in this case the target is sufficiently strong to be detected by conventional processing alone.

Fig.4 shows the range-doppler maps for a different CIT recorded less than a minute later. This CIT contained strong RFI received in the main beam from an unknown source. The RFI has obscured the target after conventional processing in Fig.4(a), but the application of STAP successfully removes much of the RFI and uncovers the target in Fig.4(b). The benefit of STAP is reflected most clearly by the comparison of Doppler spectra at the target range bin in Fig.5(b) after CFAR processing the outputs in Fig.4. Note that while the target cannot be detected by conventional processing, it can be easily seen 18 dB above the noisefloor when STAP is applied.

5. CONCLUSIONS

A practical STAP method was described for joint sidelobe and range-correlated mainlobe disturbance cancellation using filters of relatively low dimension. The judicious selection of spatial and temporal degrees of freedom permits suitable training data to be found and keeps the computational load at modest levels for real time implementation. These aspects are also important for other radar systems [6].

The proposed STAP technique cancelled clutter-plus-noise to improve the effective SNR at the threshold detection circuit by approximately 6 dB relative to conventional processing. This improvement was representative for the data set in CIT not containing strong RFI. When strong RFI was present, it was found that STAP could detect the known target with an effective SNR of 18 dB while conventional processing failed to see the target. This advantage may be critical in stressing environments when frequency changes are not practical and strong RFI threatens to preclude target detection.

6. REFERENCES

[1] G.J. Frazer, "SkyLOS - OTH radar augmentation using a line-of-sight receiver system," *Discussion Paper*, DSTO-DP-0928, Defence Science and Technology Organization, Australia, 2003.

[2] A. Farina, G.A. Fabrizio, W.L. Melvin, and L. Timmoneri, "Multichannel array processing in radar: state of the art, hot topics and way ahead," *in Proceedings Sensor Array and Multichannel Signal Processing Workshop (invited paper)*, IEEE, 2004.

[3] M. Turley and M.L. Lees, "An adaptive impulsive noise suppressor for FMCW radar," *in Proceedings IREECON'87*, 21st International Electronic Convention and Exhibition, Sydney, Australia, pp. 665-668, 1987.

[4] R. Klemm, "Applications of space-time adaptive processing", The Institution of Electrical Engineers, 2004.

[5] I.S. Reed, J.D. Mallet and L.E. Brennan, "Rapid convergence rate in adaptive arrays," *IEEE Transactions on Aerospace and Electronic Systems*, Vol.10, No.6, pp. 853-863, 1974.

[6] G.A. Fabrizio, L.L Scharf, A. Farina, and M.D. Turley, "Ship detection with HF surface wave radar using short integration times," *in Proceedings of the International Radar Conference*, IEEE, 2004.

(a) Result 1

Fig. 1. The Westwind (PEL-AIR) cooperative aircraft target.

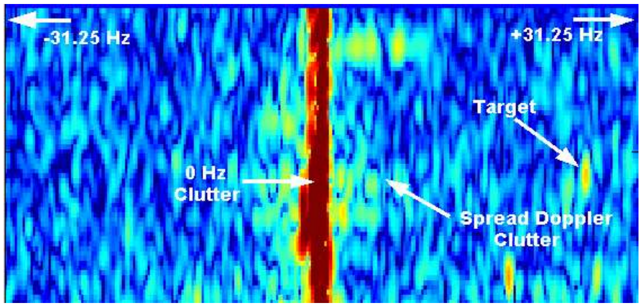

(a) Range-Doppler map for beam steered in target direction.

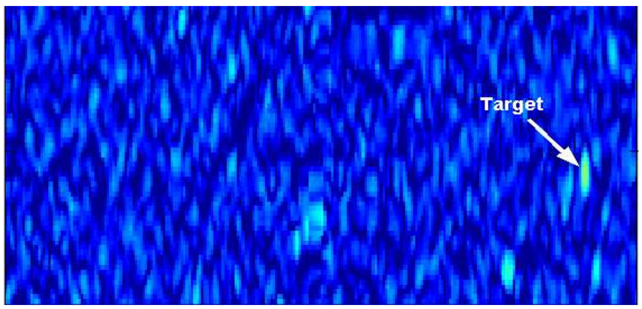

(b) Range-Doppler map after cell averaging CFAR processing.

Fig. 2. Conventional output for CIT without strong RFI.

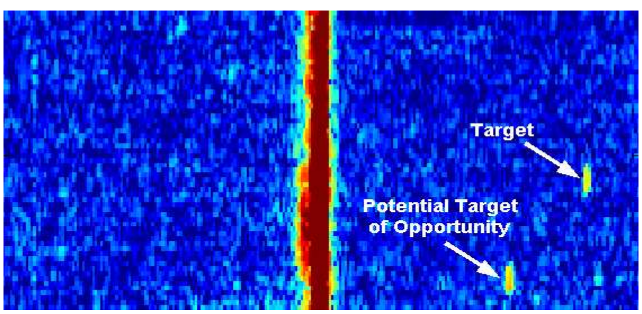

(a) Range-Doppler map for beam steered in target direction.

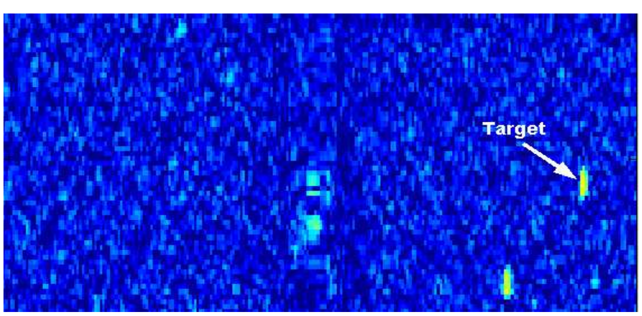

(b) Range-Doppler map after cell averaging CFAR processing.

Fig. 3. STAP output for CIT not containing strong RFI.

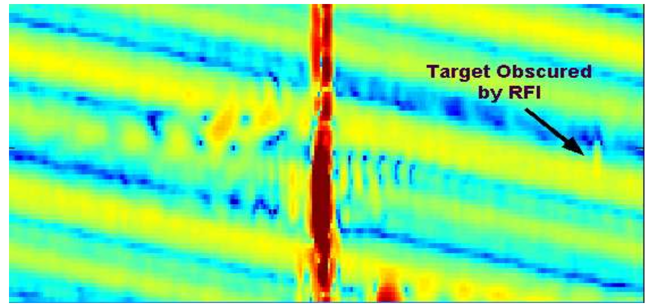

(a) Conventional range-Doppler map in target beam.

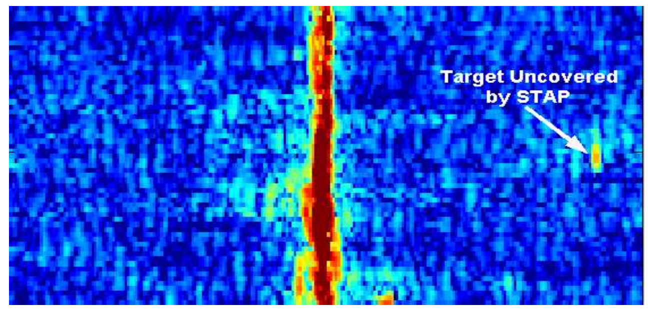

(b) STAP range-Doppler map in target beam.

Fig. 4. STAP and Conventional outputs with strong RFI

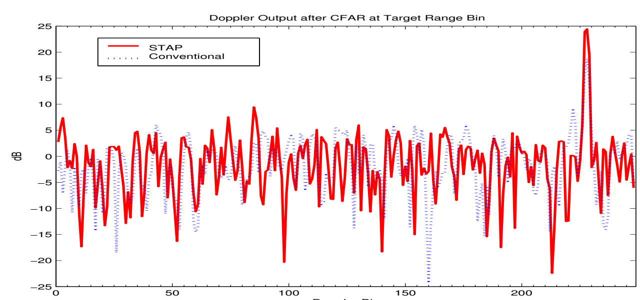

(a) CIT not containing strong RFI.

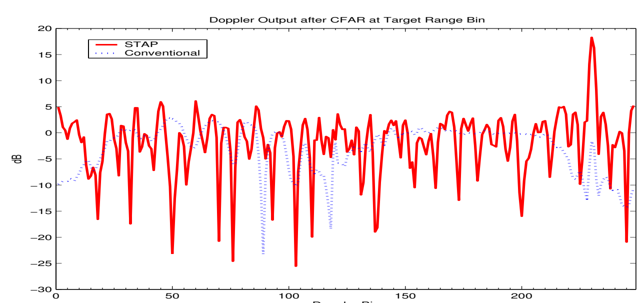

(a) CIT containing strong RFI.

Fig. 5. Conventional and STAP Doppler spectra after CFAR.